Chemical Science

ROYAL SOCIETY OF CHEMISTRY

EDGE ARTICLE

View Article Online
View Journal | View Issue

Cite this: *Chem. Sci.*, 2025, **16**, 3157

All publication charges for this article have been paid for by the Royal Society of Chemistry

Innocuous solvent-based, low-temperature curable, and highly transparent photosensitive polyimides developed using soluble polyimides containing bio-based magnolol moieties†

Huifa Meng,[ab] Kaijin Chen,[b] Chuying Li,[b] Longfei Zhang,[c] Yanwei He,[d] Zining Zhao,[b] Peixin Wu,[b] Hai Zhu,[c] Zhenguo Chi,[e] Jiarui Xu,[b] Siwei Liu[b] and Yi Zhang *[ab]

Traditional photosensitive polyimide (PSPI) materials require a high curing temperature and exhibit low transparency, limiting their applications in thermally sensitive optical devices. To overcome this challenge, soluble photosensitive polyimide resins were synthesized based on the structural design of a bio-based magnolol monomer. It is noteworthy that the PI photoresist, developed by using the as-prepared polyimides and non-toxic solvents (2-acetoxy-1-methoxypropane, PGEMA) and other additives, demonstrated an impressive low-temperature curing performance (180 °C). Furthermore, the solvent residue in the cured film prepared using PGEMA as solvent was markedly decreased compared to that prepared using *N*-methyl pyrrolidone (NMP). In addition, the **C-PI-3** films cured by photoinitiated thiol–ene radical reactions exhibited high transparency with an average visible light transmittance of 87.8%, as well as excellent thermal stability, dielectric and breakdown properties, and photo-patterning capabilities. This partially bio-based and innocuous solvent-based PSPI with low-temperature curability and high transparency properties could be a pioneering example to resolve the challenges of energy efficiency and environmental sustainability and is expected to be used in the field of color filters.

Received 24th November 2024
Accepted 4th December 2024

DOI: 10.1039/d4sc07952c

rsc.li/chemical-science

Introduction

Photosensitive polyimide (PSPI) is a key material with a wide range of applications in the fields of semiconductors, microelectronics, and display devices, due to its excellent mechanical, thermal, dielectric, and lithographic properties.[1–4] In recent years, there has been considerable interest in the development of cured PSPI films with high optical transparency in the visible range for use in flat-panel electronic displays and optical devices, such as color filters (CFs).[5–8] Although the introduction of fluorine-containing monomers can effectively improve the optical transparency of PSPI films, the problem of the high temperature (above 350 °C) imidization process remains unresolved.[9] It is evident that processing at such elevated temperature has some detrimental impacts. It is possible that some of the indispensable components of the photoresist may undergo thermal decomposition, or that certain substrates utilized in temperature-sensitive devices may be incapable of withstanding the requisite curing temperatures.[10]

It is understandable that the design of new PSPI, which features low curing temperatures (≤200 °C) and high optical transparency, is attractive and can contribute to energy efficiency. In many studies of negative-tone PSPI (n-PSPI), alkaline catalysts (*e.g.*, heteroaromatic-based,[11] photo-based generators,[12,13] or thermal-based generators[14]) have been employed to efficiently reduce the energy barrier of the reactions, enabling the precursors of PSPI to be cured at a low temperature. Another alternative is to use diamine monomers with heteroaromatic groups to facilitate the preparation of low-temperature curable n-PSPI films.[15] Nevertheless, the incorporation of an excessive number of heterocycles may have an inevitable impact on the optical characteristics of normal polyimide films.[16] Besides, the precursors of polyimides, which are always used as matrix resins in these instances, must undergo structural or chemical transitions to achieve the desired properties. This process entails the generation of water vapor or the disruption of the

[a]*School of Chemical Engineering and Technology, GBRCE for Functional Molecular Engineering, IGCME, Sun Yat-sen University, 519082 Zhuhai, China*

[b]*PCFM Lab, GD HPPC Lab, Guangdong Engineering Technology Research Centre for High-performance Organic and Polymer Photoelectric Functional Films, State Key Laboratory of Optoelectronic Materials and Technologies, School of Chemistry, Sun Yat-sen University, Guangzhou 510275, China. E-mail: ceszy@mail.sysu.edu.cn*

[c]*School of Physics, Sun Yat-sen University, Guangzhou 510275, China*

[d]*Wuxi Shunxuan New Materials Co., Ltd, Wuxi 214037, China*

[e]*School of Environmental and Chemical Engineering, Wuyi University, Jiangmen, 529020, China*

† Electronic supplementary information (ESI) available. See DOI: https://doi.org/10.1039/d4sc07952c

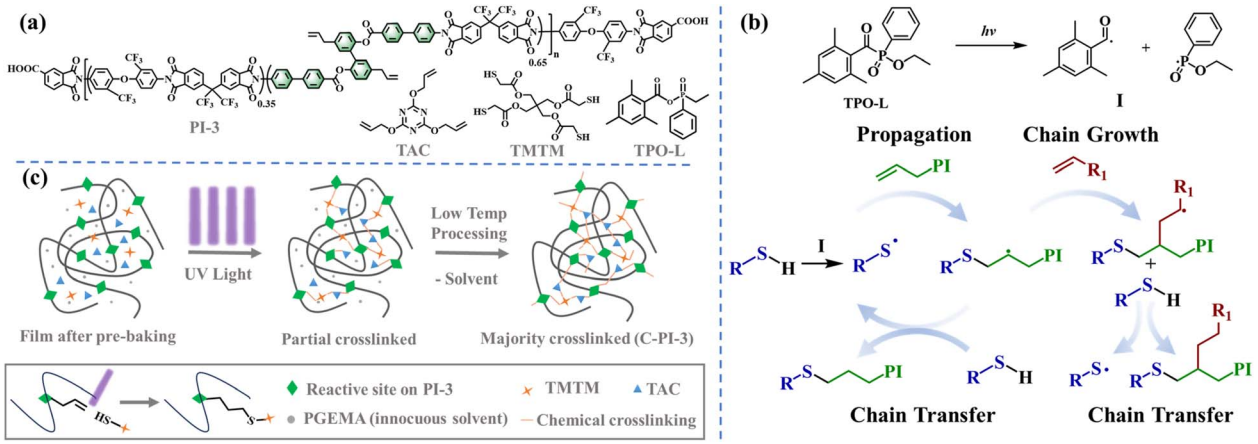

Fig. 1 (a) The main compositions of the PI-3 photoresist, (b) the reaction mechanism of the thiol–ene reaction, and (c) the reaction scheme.

bond between the PI and the crosslinking network, which can give rise to defects and shrinkage in the films.[17]

Another promising approach is to utilize soluble PI as the matrix for PSPIs, obviating the necessity for further intramolecular cyclisation during the hardbake process.[18,19] However, soluble PIs with high transmittance often lack photo-crosslinking groups, which poses a challenge in developing efficient photo-crosslinking processes for photopatterning. Furthermore, the process temperature is primarily concerned with the complete removal of the casting solvent, with the aim of ensuring reliability. The commonly used solvents for PSPI solutions are *N*-methyl pyrrolidone (NMP) and 1,4-butyrolactone (γ-GBL).[20–22] However, both have boiling points exceeding 200 °C, which renders the removal of casting solvents from the films more challenging at a lower process temperature (≤200 °C).[17] Additionally, it is important to note that NMP has the potential to pose health risks.[23] Consequently, the development of PSPI systems utilizing soluble PIs with efficient photosensitive groups, and innocuous green solvents with low boiling points represents an inevitable trend.

Photoinitiated thiol–ene radical reactions represent an efficient and rapid ligation reaction, providing a powerful approach for the fabrication of multi-functional materials through chemical synthesis,[24,25] 3D printing,[26] lithographic patterning,[27–29] and other techniques.[30] Thiol–ene-based photoresists possess the advantage over their meth(acrylate)-based counterparts of being relatively insensitive to oxygen inhibition.[26] Consequently, this circumvents the necessity for exposure in an inert environment and permits the utilization of low light intensities. Furthermore, the demand for olefins extends beyond methacrylates to include vinyl ethers, allyl, and alkynyl groups, which are also applicable in light-triggered thiol–ene radical reactions.[31–33] Owing to these advantages, several innovative petroleum-based or bio-based olefinic monomers have been developed and investigated in previous studies to enhance the properties of polyimides through thiol–ene reactions.[34–36]

Magnolol is a natural and safe product extracted from the bark of *Magnolia officinalis*.[37] The inherent biphenyl–bisphenol structure of this compound exhibits low symmetry, thereby enabling the synthesis of aromatic resins with low regularity through feasible designs. Besides, the appended allyl groups can serve as the reaction sites for the preparation of high-performance resins through the light-triggered thiol–ene reaction. In this work, a novel partially bio-based diamine monomer (DDBA) was synthesized from magnolol, and polymerized with commercially available monomers to prepare soluble polyimide resins. Noteworthily, the preparation of these soluble polyimides can circumvent the complicated synthesis process of traditional photosensitive poly (amic ester) precursors (PAEs), which are used as the matrix for PSPIs.[9] Subsequently, the polyimide photoresists were developed using the combinations of the as-synthetic polyimide resins containing allyl groups, photoinitiators, crosslinkers containing sulfhydryl or allyl ether, and non-toxic solvents (PGEMA) (Fig. 1a). A reliable approach to photopatterning of photosensitive polyimides was achieved through the photoinitiated thiol–ene radical reaction, expanding an available way to obtain the new PSPI with excellent comprehensive properties and high pattern resolution (Fig. 1b and c).[38] The outgassing, transparency, thermal stability, dielectric and breakdown properties, and photo-patternable capabilities of the as-prepared PSPI films cured at a low temperature (180 °C) were investigated through a series of characterization experiments. This work presents a novel strategy for the development of bio-based photosensitive polyimides with good solubility in non-toxic solvents, superior low-temperature curing performance, and exceptional lithographic capabilities. This strategy may broaden the potential applications of bio-based photosensitive polyimides with high performances in the fields of optoelectronics and semiconductors and is also aligned with the contemporary trend of green and sustainable development.

Experimental

Materials

4,4′-(Hexafluoroisopropylidene) diphthalic anhydride (6FDA) and 2,2′-bis(trifluoromethyl)-4,4′-diaminodiphenyl ether (6FODA) were supplied by China Tech (Tianjin) Chemical Co., Ltd and used as received. 2,4,6-Triallyloxy-1,3,5-triazine (TAC),

pentaerythritol tetrakis(2-mercaptoacetate) (TMTM), dicumyl peroxide (DCP), (4-aminophenyl)boronic acid hydrochloride, ethyl(2,4,6-trimethylbenzoyl) phenylphosphinate (TPO-L), 4-bromobenzoyl chloride, magnolol, and 2-acetoxy-1-methoxypropane (PGMEA) were purchased from Aladdin Industrial Corporation. Tripotassium orthophosphate (K_3PO_4) triethylamine (TEA), tetrakis(triphenylphosphine)palladium ($Pd(PPh_3)_4$), trimellitic anhydride, and 2-(*tert*-butyl)-4,6-dimethylphenol (TBX) were obtained from Bidepharm. *N*-methylpyrrolidone (NMP), tetrahydrofuran (THF), *N*,*N*-dimethylacetamide (DMAc), dichloromethane (DCM), ethyl acetate (EA), *N*-vinyl-2-pyrrolidinone (NVP), and pyridine (Py) were bought from J&K Scientific and used as received. All other common solvents were of analytical grade and used without further purification.

Synthesis of 5,5′-diallyl-[1,1′-biphenyl]-2,2′-diyl bis(4′-amino-[1,1′-biphenyl]-4-carboxylate) (DDBA) and its intermediate products

The detailed synthetic procedure and characterization are illustrated in the ESI.†

Preparation of polyimide resins

The polyimides were prepared by a two-step process. Taking **PI-2** as an example, to a solution of DDBA (5.0000 g, 7.61 mmol) and 6FODA (2.5596 g, 7.61 mmol) dissolved in anhydrous NMP solution (57 mL), trimellitic anhydride (0.3655 g, 1.90 mmol) and 6FDA (6.3410 g, 14.27 mmol) were added to obtain a solution with a solid content of approximately 20 wt%. After stirring for about 12 h at room temperature under argon conditions, a poly(amide acid) (PAA) glue was obtained. Subsequently, acetic anhydride (4.02 mL) and pyridine (1.73 mL) were added. After stirring for the next 24 h, the mixed solution was precipitated in 2 L of deionized water and ethanol (7/3, V/V) and washed three times with ethanol. Finally, the above precipitate was dried at 80 °C under vacuum to obtain the PI powders.

Similarly, other PI resins were prepared using the same method to **PI-2** resins, except that the molar ratio of DDBA/6FODA was changed, resulting in **PI-1**(0/100), **PI-2**(50/50), **PI-3**(65/35), and **PI-4**(80/20), respectively.

Photopatterning of PSPI films

In a 100 mL flask equipped with a magnetic stirrer, synthetic PI resins (10.00 g) were dissolved in PGEMA (20.55 g). Then, TPO-L (0.40 g), antioxidant TBX (0.08 g), TAC (1.00 g), TMTM (0.90 g) and DCP (0.30 g) were dissolved with stirring for 8 h to obtain a homogeneous solution at about 30 wt% concentration. The above solution was filtered through a 2 μm Teflon filter prior to use.

The PSPI solutions were coated onto a silicon wafer at room temperature and then soft baked at 70 °C for 2 min. The wafer was maskless exposed to 380 nm light with an exposure time of 200 ms. Substrates can be developed with PGEMA (24 s) and rinsed in ethyl alcohol (10 s) at about 25 °C to obtain the photopattern of PI films. Finally, the wafer was baked in a low temperature process at 180 °C for 1 h in a nitrogen environment to remove the residual solvents. The cured PI films were named **C-PI-1**, **C-PI-2**, and **C-PI-3**, according to the soluble polyimide resin used.

Results and discussion

Synthesis and characterization of the polyimide resins

The diamine monomer (DDBA) was accessed from the bio-based monomer magnolol in decent yields. The synthetic routes and specific characterization results are detailed in Fig. 2a, S1 and S10 (ESI).† The general synthetic route for the partially bio-based polyimides is illustrated in Fig. 2b. Four types of polyamide acid solutions (PAAs) were prepared by polymerizing commercially available dianhydride 6FDA with diamines, tailoring the feed molar ratios of DDBA and 6FODA monomers. Meanwhile, trimellitic anhydride was used as an end-capping agent to control the molecular weight. The obtained PAAs were then chemically imidized by mixing acetic anhydride with pyridine. The successful synthesis of the partially bio-based PI resins was confirmed by FT-IR and NMR analysis (Fig. S11 and S16, see the ESI for details†). Traditional photosensitive PAEs were developed using anhydride and alcohol with the photosensitive group forming a diacid diester, which subsequently reacted with a diamine after acyl chlorination.[9,11] Different from the traditional complicated synthesis process of photosensitive PAEs, the process for the preparation of these bio-based polyimides, containing allyl groups (serving as the photosensitive group), is relatively mild.

The poor solubility and processability of conventional rigid polyimides have severely limited their wide applications. This is due to the tighter chain stacking of these materials, which prevents solvent molecules from penetrating. The incorporation of low-polarity fluorine atoms or monomers with large steric hindrance has been demonstrated to be an efficacious approach for improving the solubility of polyimides.[39] Given that DDBA is a fluorine-free diamine monomer, it is essential to investigate its molecular planarity prior to conducting a dissolution experiment on synthetic polyimide resins. The theoretical calculation demonstrated that DDBA displayed more non-coplanar characteristics than 6FODA (Fig. S17, ESI†). Reasonably, all samples in this work were found to be soluble in common organic solvents (*e.g.* NMP, DMAc, THF, and DCM), and even NVP, a reactive diluent for the solvent-free preparation of photocurable resins[40] (Table S1†). Specifically, all the samples except **PI-4** were soluble in PGEMA and EA (non-toxic solvents) at room temperature. This result is encouraging for the development of polyimide coatings using environmentally friendly and innocuous solvents. Therefore, the following series of discussions will focus on polyimide coatings with the PGEMA-based solvent.

To investigate the impacts of different backbones on the chemical functionalization and various physical properties of the as-prepared PIs, the number-average molecular weight (M_n) of all PIs was controlled at about 2.5×10^4 g mol^{-1}. M_n was measured in the range of $2.77–3.02 \times 10^4$ g mol^{-1} with the polydispersity indices (PDI) between 1.32 and 1.34 (Table S1†). The intrinsic viscosity (η) of the synthetic polyimides spanned

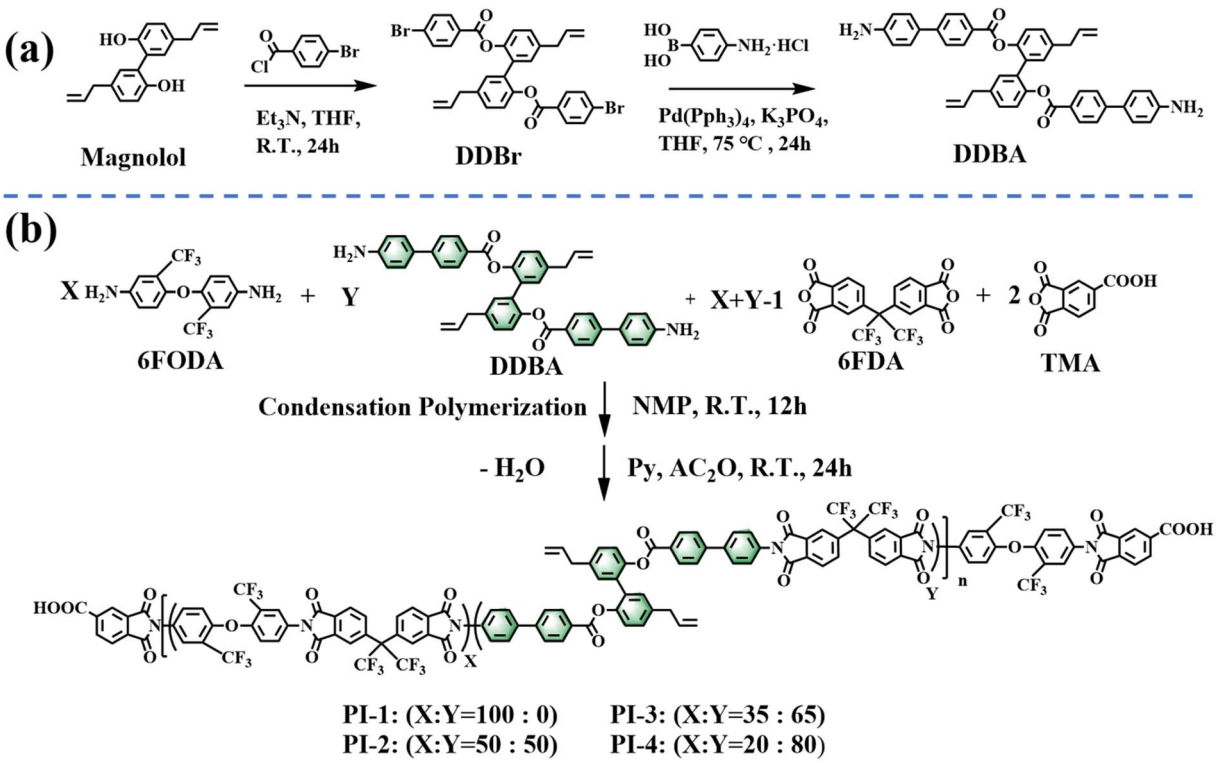

Fig. 2 Synthetic routes of (a) DDBA and its intermediate products and (b) polyimides.

the range of 0.25–0.35 dL g^{-1} (Table S1†). Such a low η of the PI solution minimizes loss during filtration, facilitates good spreading and wettability during the spin-coating process, and enhances the formation process to improve film quality.

Preparation and characterization of the cured PSPI films

The PSPI solutions were prepared by combining the soluble PI resins, innocuous solvent (PGEMA), photoinitiators, crosslinkers, and other additives in a certain ratio. The lithographic patterning of the PSPI films was obtained by photoinitiated thiol–ene radical reactions, after which the UV-exposed films were baked at 180 °C for one hour to remove the residual solvent and to carry out further crosslinking. The C=C double bond, with a specific absorption at approximately 1637 cm^{-1} in FT-IR spectroscopy, can be monitored to determine the extent of the reactions.[29] As shown in Fig. S18a (ESI),†

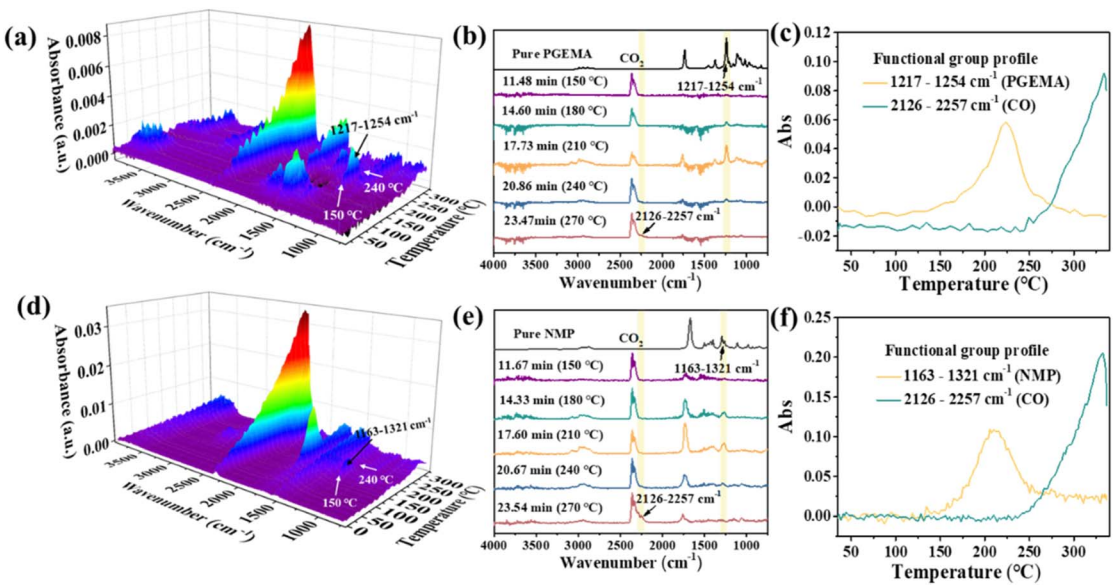

Fig. 3 Three-dimensional FT-IR spectra, the corresponding absorption spectra, and the functional group profiles (FGP) of the escaping gas during heating processes: the **PI-3** used (a–c) PGEMA and (d–f) NMP as solvents after curing at 180 °C for 1 h.

the absorbance of C=C of **C-PI-3** decreased dramatically after exposure and almost disappeared after further heating, confirming the formation of the cross-linked network structure. The results were further supported by the chemical resistance of the cured PSPI films. As shown in Table S2,† **C-PI-2** and **C-PI-3** had no obvious thickness change before and after the chemical resistance experiment, indicating good chemical stability. In addition, the three cured PI films showed a broad peak in X-ray diffraction measurements, which indicated the amorphous structure of the C-PI films (Fig. S18b, ESI†). The above results showed that the incorporation of DDBA in soluble polyimide enabled the formation of a cross-linking structure between the **PI-3** and crosslinkers under UV exposure, which is a prerequisite for lithography.

Outgassing of the cured PSPI films

To investigate the components escaping from the UV-exposed wet film of **C-PI-3** during the post-drying stage (180 °C), thermogravimetry-infrared (TG-IR) measurement was carried out with a heating rate of 10 °C min^{-1} and kept at 180 °C for 1 h under a nitrogen atmosphere. The three-dimensional FT-IR spectra, Gram-Schmidt (GS) curves, and functional group profiles (FGP) are shown in Fig. S19 (see the ESI for details).† The result demonstrated that only solvent (PGEMA) volatilized during the post-curing process in the UV-exposed wet film of **C-PI-3**. Noteworthily, conventional photosensitive PAEs were accompanied by the release of solvents, water or crosslinked groups during the high-temperature imidization processing,[20] which caused the cured films to shrink. In contrast, **C-PI-3** exhibited a notable low-temperature curing performance (180 °C). In this case, the absence of structural transitions in imidized **PI-3** and the retention of crosslinkers in **C-PI-3** were conducive to the production of a high-quality film.

The aim is to use the innocuous solvent PGMEA to produce PSPI solutions instead of toxic solvent NMP, which is the common solvent used in traditional PSPI solutions. To compare the solvent residue, we used both PGEMA and NMP to separately dissolve **PI-3** resin and other additives to prepare PSPI solutions, abbreviated as the PGEMA system and the NMP system. Then, both the UV-exposed wet films were kept in an oven at 180 °C in a nitrogen atmosphere for 1 h, after which the TG-IR experiments were carried out from room temperature to 330 °C at a rate of 10 °C min^{-1}. In Fig. 3a and d, both three-dimensional FT-IR spectra showed the characteristic absorption of the H_2O and CO_2 before 150 °C due to the test environment and the water absorption of the cured films. However, new absorption peaks were found simultaneously in both systems when the temperature was above 150 °C, and the corresponding absorption spectra of the escaping gas are partially shown in Fig. 3b and e. There was a good correspondence between the absorption spectra of the escaping gas at 210 °C and that of the pure PGEMA. Subsequently, the FGP curves determined using the wavenumbers of the region between 1217 and 1254 cm^{-1} can be used to show that the escape of PGEMA occurred in the temperature range of 150 °C to 240 °C (Fig. 3c). Besides, the absorption peaks between 2126 and 2257 cm^{-1} appeared at 270 °C, corresponding to the specific absorption of CO. According to the FGP curves determined using the above wavenumbers, it was found that this absorption occurred after approximately 240 °C, indicating the onset of thermal decomposition. In conjunction with the analysis of FGP curves, the GS curves can be divided into two parts (Fig. S20a, ESI†). The initial peak observed between 150 °C and 240 °C can be attributed to the absorption peaks of PGEMA, while the subsequent peak occurring at temperatures exceeding 240 °C was indicative of the absorption of decomposition products. Similarly, the NMP system can also be analyzed using the above approach. The difference in the results for the NMP system is that the initial peak in the GS curves was due to the absorption of NMP gas (Fig. S20b, ESI†).

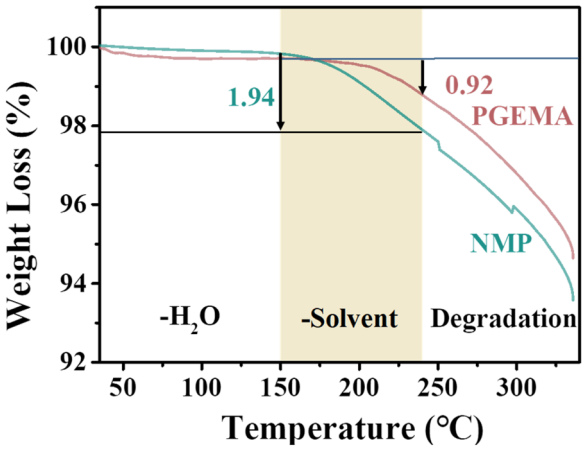

Fig. 4 The TGA curves of **C-PI-3** prepared using different solvents after curing at 180 °C for 1 h (red: PGEMA and green: NMP).

Thereby, the process of weight loss can be divided into three main parts [I] – (35–150 °C), [II] – (150–240 °C) and [III] – (240–330 °C) in the TGA curves (Fig. 4). The weight loss of the sub-process [I] was attributed to the desorption of water from the films. The sub-process [II] corresponded to the weight loss of the residual solvent of the films, while both films began thermal decomposition at above 240 °C. The residual solvents in the PGEMA system can be calculated to be approximately 0.92 wt% by weight, and in the NMP system, around 1.94 wt%. The results indicated that higher reliability of the cured films was achieved in the PGEMA system after the low temperature process.

Optical properties

In contrast to conventional photosensitive PAEs, the imidized photosensitive PI resin does not necessitate a high-temperature post-curing procedure, which is pivotal to prevent any deterioration in optical properties of the cured films. As shown in Fig. 5a and Table S1 (ESI),† the cut-off wavelength (λ_0) and average visible light transmittance (AVT) from 400 to 780 nm of the PI films with 9 ± 1 μm thickness were 323–342 nm and 89.2–92.9%, respectively. The transparency of PI is enormously influenced by intramolecular and intermolecular charge transfer interactions (CTC).[41] To gain further insights into the influence of intramolecular CTC, time-dependent density

Table 1 Optical and thermal properties of the cured PSPI films

Sample	λ_0[a] (nm)	AVT[b] (%)	T_g[c] (°C)	CTE[d] (ppm K^{-1})	E'[e] (MPa)	νe (mol cm^{-3})	T_{d5}[f] (°C)	Char yield[g] (wt%)
C-PI-1	335	89.7	274	72.20	2.8	—	326	38.9
C-PI-2	342	87.3	272	70.64	43.6	1.6×10^{-3}	354	42.7
C-PI-3	341	87.8	284	61.82	162.3	5.8×10^{-3}	371	45.8

[a] Cut-off wavelength. [b] Average visible light transmittance (400–780 nm) of PSPI films with 12 ± 1 μm thickness. [c] Glass transition temperature was determined from the maximum tan delta values in DMA tests at a heating rate of 3 °C min^{-1}. [d] Coefficient of thermal expansion (CTE) ranging from 50 to 180 °C was calculated by TMA at a heating rate of 10 °C min^{-1}. [e] Storage modulus at the viscous state, measured by DMA at the temperature of T_g + 40 °C. [f] Measured by TGA with 5% weight loss in nitrogen. [g] Residual weight percentage at 800 °C was measured by TGA in nitrogen.

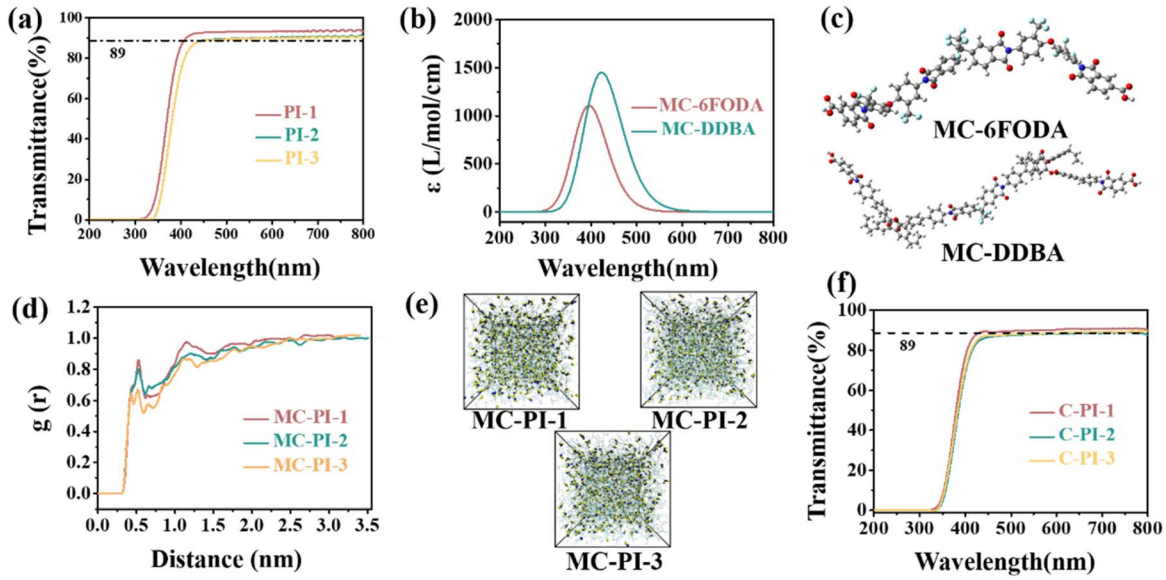

Fig. 5 (a) UV-vis spectra of the PI films, (b) the simulated absorption spectra of model compounds, (c) the molecular models of MC-6FODA and MC-DDBA, the repeating unit was terminated with trimellitic anhydride (gray, white, red, blue, and cyan balls represent C, H, O, N, and F atoms, respectively), (d) the RDFs between one selected N atom of the imide ring and all C atoms of the carbonyl groups, (e) polymer simulation models of MC-PI-1, MC-PI-2, and MC-PI-3, and (f) UV-vis spectra of the cured PSPI films.

functional theory (TD-DFT) calculations were performed on the model compounds, abbreviated as MC-6FODA and MC-DDBA, in order to obtain the simulated UV-vis absorption curves (Fig. 5b, c and Table S3†). The results demonstrated that MC-6FODA showed absorption peaks at shorter wavelengths in comparison to MC-DDBA, indicating that the former displayed a weaker intramolecular CTC. Subsequently, the calculations of radial pair distribution functions (RDFs) were carried out to investigate the impact of intermolecular CTC.[42,43] Fig. 5d and e illustrate the temporal development of the C–N distances for one selected N atom of the imide ring and all C atoms of the carbonyl groups, and polymer simulation models of MC-PI-1, MC-PI-2, and MC-PI-3. The MC-PI-1 model represented 10 chains of **PI-1** with 30 repeating units, terminated with trimellitic anhydride, which were randomly positioned within a cubic box. The mean density of the C atoms on the carbonyl group within the box was observed to decrease with the replacement of 6FODA by DDBA within 0.75 nm distance of the selected N atoms (directly connected N–C combinations have been excluded). To further elucidate, the incorporation of DDBA monomers with relatively non-coplanar structures can potentially loosen chain packing and diminish the intermolecular CTC between PI chains. In other words, 6FODA improves the light transmittance of PI through the electron absorption effect, while DDBA affects the transparency through the increase in free volume caused by the stereoscopic effect. The experimental results demonstrated that the transmittance decreases slightly with the increase of DDBA, so the electronic effect is greater than the stereoscopic effect.

Nevertheless, the transparency of the cured PSPI films was somewhat inferior to that of the resin itself, with the AVT ranges of 87.3–89.7% (Fig. 5f and Table 1). This discrepancy may be attributed to the formation of by-products after the decomposition of the initiator. In short, the low-temperature curable PSPI films displayed excellent optical transparency, demonstrating compatibility with thermally sensitive and optical devices.

Thermal properties and dimensional thermal stability

Thermal stability, dimensional stability and thermomechanical properties are the most essential properties for polyimide films

used in electronics and other applications where the films are subjected to extensive temperature excursions.[44] As illustrated in dynamic mechanical analysis (DMA) thermograms (Fig. 6a and b), the storage modulus at the viscous state (E') of **C-PI-1** was close to 0 MPa, which was attributed to the plasticizing effect of an aliphatic thioether structure blended into the PI phase without interaction. However, the storage modulus of **C-PI-2** and **C-PI-3** exhibited a rubbery plateau with approximate values of 43.6 MPa and 162.3 MPa, respectively. The above results indicated that the concentration of covalent bonds was the highest in **C-PI-3**, while the non-bonding interaction became weak at such high temperature.[45] As shown in Table 1, the calculated cross-linking density (νe) of **C-PI-3** was higher than that of **C-PI-1** and **C-PI-2**, resulting in the highest T_g (284 °C) among the cured PSPI films.

As the concentration of crosslinking combinations between the polyimide and crosslinkers increased, the values of the coefficient of thermal expansion (CTE) dropped from 72.20 to 61.82 ppm K^{-1}, representing a decrease in CTE of about 17% (Fig. 6c and Table 1). The obvious decrease was attributed to the constraints of the main PI backbones passing through the crosslinking reactions.[46] As illustrated in the TGA curves (Fig. 6d), the volatiles before 400 °C are any thermally degraded products from crosslinkers and photoinitiators in addition to water and solvents. This is particularly significant for polyimides cured in a low temperature process. The decomposition temperature at 5% weight loss (T_{d5}) of the cured PSPI films was found to be 326–371 °C. The results demonstrated that the thermal stability of cured PSPI films was improved when the polyimide participated in the formation of the crosslinking network. Furthermore, a significant difference in the DTG curves of the samples was observed up to 400 °C. This was mainly attributed to the fact that in **C-PI-3** with higher νe, more aliphatic crosslinkers were connected to the aromatic backbone by chemical bonds, delaying the thermal degradation and making the release of these thermal decomposition products more difficult.[47]

Water absorption, electrical and mechanical properties

The water absorption and electrical properties of PSPI insulating materials are important to guarantee the efficiency and long-term reliability of optical devices. The values of saturated water absorption capacity at 95% RH and 25 °C are listed in Table 2, in the range of 1.27% to 1.62%. Meanwhile, the cured PSPI films also exhibited satisfactory dielectric properties, which were due to the low water absorption. The dielectric factor (D_f) values of the cured PI films at 10 GHz (50% RH, 25 °C) were found to be 0.0095–0.0103, and the dielectric constants (D_k) were less than 3.0 (Table 2). The water absorption and dielectric properties of the cured PSPI films were inextricably linked to the chemical structure and the aggregation form of molecular chains (see Fig. S21a and b, ESI for details†). Nevertheless, despite the inclusion of polar additives, the low-temperature cured films in this study exhibited a diminished capacity for water absorption and a comparable dielectric

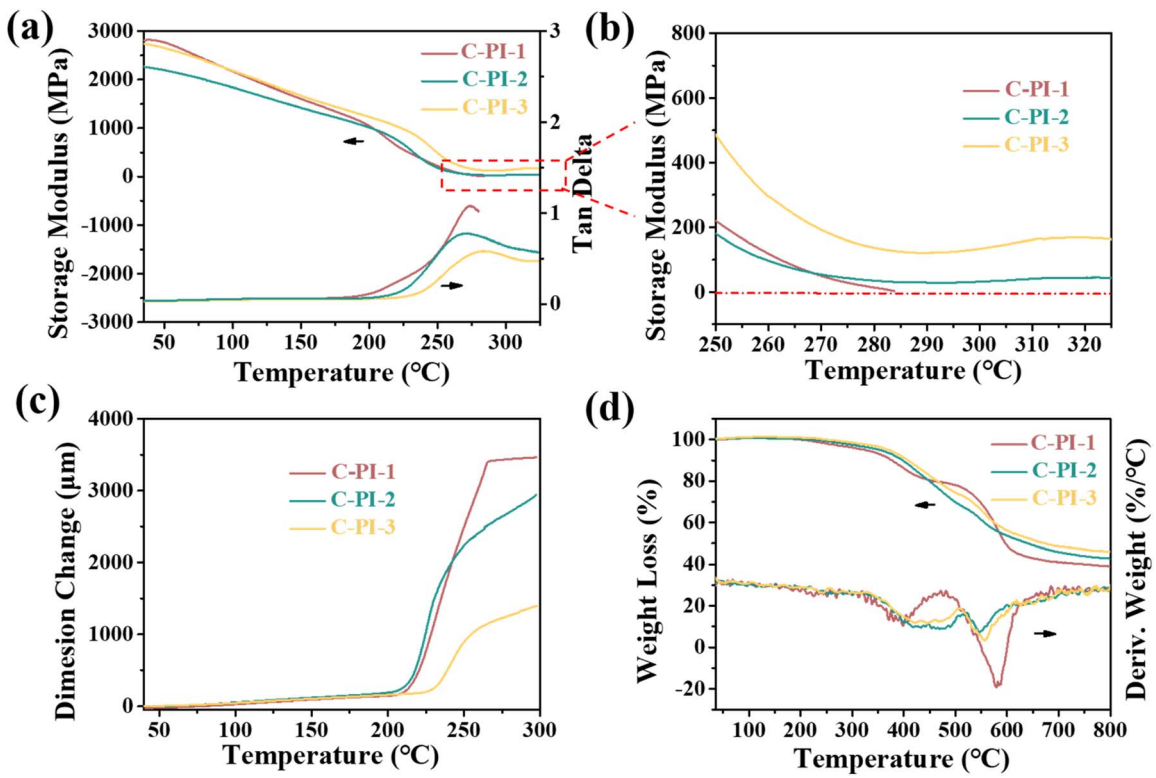

Fig. 6 (a) DMA curves (storage modulus and tan delta *versus* temperature), (b) zoomed-in regions of DMA curves, ranging from 250 °C to 330 °C, (c) TMA curves, and (d) TGA and DTG curves of the cured PSPI films.

Table 2 Water absorption, electrical and mechanical properties of the cured PSPI films

Sample	Water absorption[a] (%)	Dielectric properties at 10 GHz[b]		Breakdown strength[c] (kV mm^{-1})	Tensile strength (MPa)	Tensile modulus (GPa)	Elongation at break (%)
		D_k	D_f				
C-PI-1	1.27	2.90	0.0095	283	102.0 ± 6.9	2.8 ± 0.2	4.8 ± 0.5
C-PI-2	1.62	2.90	0.0103	358	97.4 ± 6.8	2.3 ± 0.1	6.9 ± 0.8
C-PI-3	1.46	2.93	0.0096	381	92.1 ± 3.3	2.0 ± 0.1	7.1 ± 0.8

[a] Maximum water absorption was measured by the gravimetric method on vacuum & dynamic vapor/gas sorption equipment and was recorded at 95% RH, 25 °C. [b] Measured at 50% RH, 25 °C. [c] Measured by AC at room temperature in silicone oil.

property profile when compared to partially non-photosensitive PI films.[48,49] As shown in Table 2 and Fig. S21c,† Weibull breakdown strength (E_b) increased dramatically at room temperature from 283 kV mm^{-1} for **C-PI-1** to 358 and 381 kV mm^{-1} for **C-PI-2** and **C-PI-3**, respectively. The enhancement of breakdown strength was attributed to the intermolecular crosslinking structure between PI modified by allyl side groups and the curing agents in **C-PI-2** and **C-PI-3**, which was more conducive to decreasing electrical conductivity.[50,51]

The tensile strength at break of the cured PSPI films was measured in the range of 92.1–102.0 MPa, the tensile modulus was 2.0–2.8 GPa, and the elongation at break was 4.8–7.1% (Table 2 and Fig. S22, ESI†). Noteworthily, the cured PI films in this study displayed comparable mechanical properties with

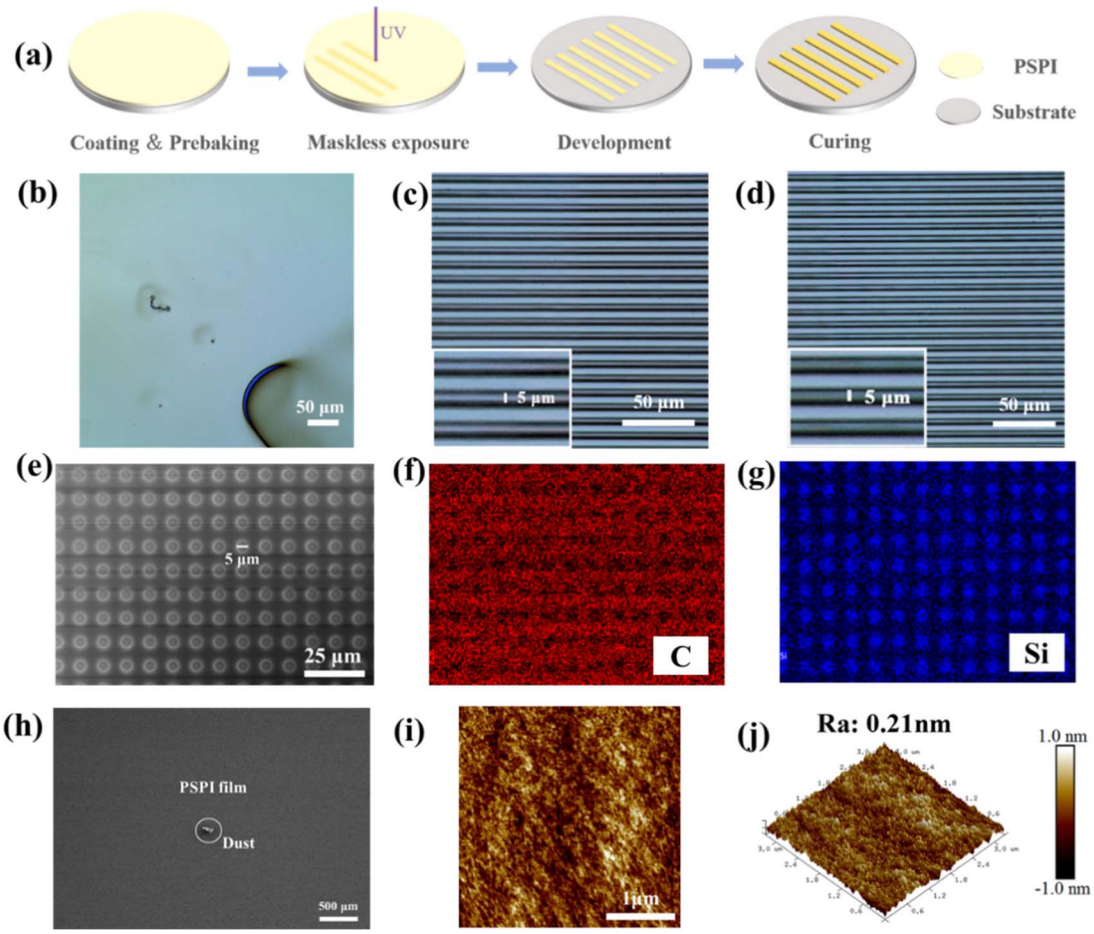

Fig. 7 Patterned thiol–ene click-based PSPI films. (a) The process of lithographic patterning. Photo images of lithographic patterns from (b) **C-PI-1**, (c) **C-PI-2**, and (d) **C-PI-3**. (e) SEM image and EDS mapping (C element (f) and Si element (g)) of the lithographic pattern from **C-PI-3**, the holes are 5 μm in diameter. (h) Surface SEM image (the dust on the PI film was selected as the focusing point), (i) planar and (j) stereogram (45°) AFM images of **C-PI-3**.

those of previously reported petroleum-based or bio-based polyimides.[52,53] This result indicated that the bio-based diamine (DDBA) possessed inherent stiffness. Moreover, **C-PI-3** with higher cross-linking density exhibited lower tensile strength, probably due to the uneven strength support of the network chains with high cross-linking site content.[46]

Photolithographic formability properties

Lithography plays an important role in the manufacture of integrated circuits and the processing of semiconductors. Photosensitive polyimide can be directly patterned and then retained on the device as the principal insulating dielectric material, which greatly simplifies the packaging process. Fig. 7a illustrates the lithography process of the negative type of PSPI. In this process, UV-exposed regions undergo chemical cross-linking through photoinitiated thiol–ene radical reactions. As shown in Fig. 1b, TPO-L is capable of absorbing light energy and subsequently cleaving to produce trimethylbenzoyl and phenyl-ethoxy-phosphonyl radicals with high initiating activity. Thiyl radicals are produced when sulfhydryl groups are affected by the above radicals. Subsequently, two different reaction cycles are possible, which involve alternation of chain transfer and propagation, as well as chain-growth mechanisms. The above mechanism is relatively insensitive to oxygen inhibition in comparison to the photo-triggered methacrylate radical reactions.[24] The cross-linking structure in UV-exposed regions can resist the effects of developer etching. Conversely, unexposed regions dissolve directly in the developing solutions. Finally, the designed pattern is obtained after a post-curing process.

Fig. 7b–d present the photo images of the lithographic patterns from the samples, which were based on the photo-initiated thiol–ene radical reactions. It was evident that the **C-PI-1** lacked a lithographic pattern, which was attributed to the absence of a cross-linked network between soluble **PI-1** and crosslinkers after UV exposure. In contrast, **C-PI-2** and **C-PI-3** with about 2.5 μm thickness showed excellent photosensitivity with a resolution of 5 μm (line). The result demonstrated that the incorporation of DDBA in soluble fluorinated polyimide enabled the achievement of its lithographic performance through photoinitiated thiol–ene radical reactions. Meanwhile, the incorporation of DDBA at a ratio of 50 mol% diamine monomers can cause substantial alterations in the solubility of the PI resins after UV exposure. Furthermore, the EDS mapping of C and Si elements showed a uniform distribution in the lithographic **C-PI-3** sample with a resolution of 5 μm (*via*), as shown in Fig. 7e–g. The surface morphology of **C-PI-3** was investigated using SEM and AFM, as illustrated in Fig. 7h–j. **C-PI-3** exhibited excellent flatness with a low roughness R_a of 0.21 nm, which facilitated the manufacture of higher chip encapsulation densities. The curing temperature and the maximum resolution of **C-PI-3** exhibited superior performance in comparison to other reported PSPI materials (Table S4†). Overall, **C-PI-3** exhibited excellent photolithographic, low-temperature curable, and high transparency properties. The results demonstrated favorable potential for the utilization of bio-based DDBA as a diamine to synthesize soluble polyimides for use in innocuous solvent-based PSPI formulations, providing a way for further advancements of innovative materials in high-performance PSPI systems.

Conclusions

In summary, a novel bio-based diamine monomer (DDBA) was successfully synthesized from magnolol, which possesses a unique asymmetric aromatic structure and a multitude of modifiable reaction sites, including phenolic and allyl groups. The DDBA was then polymerized with fluorinated monomers at different ratios to prepare three soluble polyimides (**PI-1**, **PI-2**, and **PI-3**). The partially bio-based photosensitive polyimide solutions were developed using the as-synthesized polyimides as a base, TMTM and TAC as crosslinkers, innocuous PGEMA as a solvent and TPO-L as a photoinitiator. The results of the TG-IR measurement showed that the sole ingredient (solvent, PGEMA) was volatilized from the UV-exposed wet film (**C-PI-3**) during the hardbake process. After curing at 180 °C for 1 h, **C-PI-3** exhibited a low solvent residue of 0.92 wt%, which was lower than that of the cured films in which only the PGEMA was replaced by NMP. The results showed that with the increase in DDBA diamine molar content, the comprehensive properties of the cured films were improved. **C-PI-3** exhibited high transparency (an AVT value of 87.8%), excellent thermal and electrical performances (T_g = 284 °C, D_k = 2.93, D_f = 0.0096 (10 GHz), and breakdown strength up to 380 kV mm^{-1}). Moreover, **C-PI-3** also exhibited exemplary photolithographic formability properties with a resolution of 5 μm, based on photoinitiated thiol–ene radical reactions. In short, our findings highlight the application potential of bio-based DDBA and light-triggered thiol–ene radical reactions in photolithography, providing a feasible and reliable strategy for the structural design and photopatterning approach of photosensitive soluble polyimide materials. **C-PI-3** with low-temperature curability, high transparency, and excellent photolithographic properties holds great potential as an environmentally friendly photosensitive coating material, presenting great attractiveness for employment in optoelectronics applications.

Data availability

The data supporting this article have been included as part of the ESI.†

Author contributions

Conceptualization: Huifa Meng and Yi Zhang. Sample preparation and characterization: Huifa Meng, Yanwei He, Chuying Li, Longfei Zhang, Zining Zhao, and Peixin Wu. Theoretical calculation: Kaijin Chen. Project administration: Yi Zhang and Zhenguo Chi. Writing – original draft: Huifa Meng and Yi Zhang. Writing – review and editing: all authors.

Conflicts of interest

There are no conflicts to declare.

Acknowledgements

The authors gratefully acknowledge the financial support of the projects from the Ministry of Science and Technology (No. 2022YFB3806601), National Natural Science Foundation of China (No. U20A20255, 51873239, and 52203286), Guangdong Provincial Department of Science and Technology (No. 2024B0101120001, 2020B010182001, and 2020B010179001), Guangxi Provincial Department of Science and Technology (No. AB2022035007), Basic and Applied Basic Research Foundation of Guangdong Province (No. 2022B1515020052), and Fundamental Research Funds for the Central Universities (No. 23yxqntd002). We gratefully acknowledge the TG-IR measurement in the organic and pharmaceutical analysis platform of the Instrumental Analysis & Research Center, and the maskless lithography experiment of the State Key Laboratory of Optoelectronic Materials and Technologies, Sun Yat-sen University.

Notes and references

1 M.-C. Fu, T. Higashihara and M. Ueda, *Polym. J.*, 2017, **50**, 57–76.
2 K.-i. Fukukawa and M. Ueda, *Polym. J.*, 2008, **40**, 281–296.
3 J. J. Guo, Y. Q. Bu, X. T. Li, J. Dong, X. Zhao and Q. H. Zhang, *Acta Polym. Sin.*, 2024, **55**(10), 1325–2334.
4 J. Y. Xia, N. Jiang, N. Y. Wu, X. W. Zhao, Y. M. Liu, X. W. Liu, Y. H. Hu and J. P. Lin, *Acta Polym. Sin.*, 2023, **54**, 1826–1835.
5 J. Li, Y. Yin and H. Meng, *Dyes Pigm.*, 2024, **225**, 112094.
6 Y. Gao, H. Wang, J. Jia, Z. Pan, X. Ren, X. Zhi, Y. Zhang, X. Du, X. Wang and J. Liu, *Polymers*, 2022, **14**, 3733.
7 K.-H. Kim, S. Jang and F. W. Harris, *Macromolecules*, 2001, **34**, 8925–8933.
8 G. Yu, Q. Ma, H.-Y. Chang, R. Zheng, C. Wang, L.-Y. Guo and Y.-F. Chou Chau, *Int. J. Opt.*, 2024, **2024**, 1–16.
9 J.-x. Ma, L.-l. Yuan, S.-n. Fan, L.-z. Wang, B. Jia, H.-x. Yang and S.-y. Yang, *Eur. Polym. J.*, 2023, **192**, 112071.
10 R. Okuda, K. Miyoshi, N. Arai, M. Tomikawa and G. Ohbayashi, *J. Photopolym. Sci. Technol.*, 2002, **15**, 205–208.
11 S. N. Fan, L. L. Yuan, L. Z. Wang, B. Jia, J. X. Ma, H. X. Yang and S. Y. Yang, *Polymers*, 2023, **15**, 973.
12 Y. M. Yeh, V. K. Karapala, M. Ueda and C. S. Hsu, *Polym. Adv. Technol.*, 2020, **32**, 663–669.
13 E. C. Chang, L. Y. Tseng, Y. Liu, C. K. Chen, C. C. Kuo, M. Ueda, Y. C. Lin and W. C. Chen, *J. Polym. Sci.*, 2023, **61**, 2122–2132.
14 T. Ogura, T. Higashihara and M. Ueda, *J. Polym. Sci., Part A: Polym. Chem.*, 2009, **47**, 3362–3369.
15 S. Huang, X. L. Lv, X. W. Lai, J. H. Li, Y. Zhang, S. Y. Qiu, G. P. Zhang and R. Sun, *Chem. Eng. J.*, 2023, **477**, 146858.
16 K. Xu, Z. Ke, D. Li, T. Li, G. Qian, Z. Deng, D. Li and Y. Yu, *J. Polym. Sci.*, 2024, **62**, 1808–1819.
17 Z. Karim, K. Sautter, K. Song, C. Galande and K. Singh, *International Wafer Level Packaging Conference*, IWLPC, 2020, pp. 1–6.
18 M.-H. Chen, C.-C. Lai, H.-L. Chen, Y.-H. Lin, K.-Y. Huang, C.-H. Lin, H.-T. Hsiao, L.-C. Liu and C.-M. Chen, *Mater. Sci. Semicond. Process.*, 2018, **88**, 132–138.
19 X. Jiang, H. Li, H. Wang, Z. Shi and J. Yin, *Polymer*, 2006, **47**, 2942–2945.
20 F. Windrich, E. J. Kappert, M. Malanin, K.-J. Eichhorn, L. Häußler, N. E. Benes and B. Voit, *Eur. Polym. J.*, 2016, **84**, 279–291.
21 H. Araki, Y. Kiuchi, A. Shimada, H. Ogasawara, M. Jukei and M. Tomikawa, *J. Photopolym. Sci. Technol.*, 2020, **33**, 165–170.
22 X. W. Lai, J. L. Zhang, Z. X. Yang, S. Huang, J. H. Li, G. P. Zhang and R. Sun, *Mater. Today Commun.*, 2023, **37**, 107316.
23 C. R. Kirman, B. R. Sonawane, J. G. Seed, N. O. Azu, W. T. Barranco, W. R. Hamilton, T. J. Stedeford and S. M. Hays, *Regul. Toxicol. Pharmacol.*, 2023, **138**, 105337.
24 C. Resetco, B. Hendriks, N. Badi and F. Du Prez, *Mater. Horiz.*, 2017, **4**, 1041–1053.
25 X. Chen, L. Fang, J. Wang, F. He, X. Chen, Y. Wang, J. Zhou, Y. Tao, J. Sun and Q. Fang, *Macromolecules*, 2018, **51**, 7567–7573.
26 S. C. Gauci, A. Vranic, E. Blasco, S. Bräse, M. Wegener and C. Barner-Kowollik, *Adv. Mater.*, 2023, **36**, 2306468.
27 Q. Wang, H. Cui, X. Wang, Z. Hu, P. Tao, M. Li, J. Wang, Y. Tang, H. Xu and X. He, *J. Am. Chem. Soc.*, 2023, **145**, 3064–3074.
28 C. Cao, J. Liu, X. Xia, X. Shen, Y. Qiu, C. Kuang and X. Liu, *Addit. Manuf.*, 2022, **51**, 102658.
29 H. C. Tien, X. Li, C. J. Liu, Y. Li, M. He and W. Y. Lee, *Adv. Funct. Mater.*, 2023, **33**, 2211108.
30 J. Lim, B. Goh, W. Qu, Y. Kim, J. Choi and S. Hong, *Appl. Surf. Sci.*, 2022, **571**, 151123.
31 Y. Lu, Q. Li, Z. Zhang and X. Hu, *Mater. Des.*, 2022, **224**, 111359.
32 W. Liu, P. Tian, Y. Huang and J. Zhang, *Prog. Org. Coat.*, 2022, **172**, 107125.
33 S. Mavila, J. Sinha, Y. Hu, M. Podgorski, P. K. Shah and C. N. Bowman, *ACS Appl. Mater. Interfaces*, 2021, **13**, 15647–15658.
34 H. Lee, D. Kim, S. H. Kim, Y. So, Y. H. Kim, J. Kim, J. Park, J. H. Cho and J. C. Won, *J. Mater. Chem. C*, 2023, **11**, 3459–3467.
35 S. Okamoto, A. Sudo and T. Endo, *J. Appl. Polym. Sci.*, 2021, **138**, 50529.
36 S. Xue, X. Lei, Y. Xiao, G. Xiong, R. Lian, X. Xin, Y. Peng and Q. Zhang, *Macromolecules*, 2021, **54**, 11256–11268.
37 Q. Cao, Z. Weng, Y. Qi, J. Li, W. Liu, C. Liu, S. Zhang, Z. Wei, Y. Chen and X. Jian, *Chin. Chem. Lett.*, 2022, **33**, 2195–2199.
38 B. H. Northrop and R. N. Coffey, *J. Am. Chem. Soc.*, 2012, **134**, 13804–13817.
39 M. G. Dhara and S. Banerjee, *Prog. Polym. Sci.*, 2010, **35**, 1022–1077.
40 Y. Guo, Z. Ji, Y. Zhang, X. Wang and F. Zhou, *J. Mater. Chem. A*, 2017, **5**, 16307–16314.
41 X. Jiang, Y. Long, K. Chen, Q. Yu, L. Jiang, Z. Chi, S. Liu, J. Xu and Y. Zhang, *J. Mater. Chem. C*, 2023, **11**, 1082–1094.
42 M. Brehm and B. Kirchner, *J. Chem. Inf. Model.*, 2011, **51**, 2007–2023.
43 M. J. Abraham, T. Murtola, R. Schulz, S. Páll, J. C. Smith, B. Hess and E. Lindahl, *SoftwareX*, 2015, **1–2**, 19–25.

44 R. Gao, R. Ma, J. Li, M. Su, F. Hou and L. Cao, *IEEE Trans. Compon., Packag., Manuf. Technol.*, 2022, **12**, 368–374.
45 J. Wan, B. Gan, C. Li, J. Molina-Aldareguia, E. N. Kalali, X. Wang and D.-Y. Wang, *Chem. Eng. J.*, 2016, **284**, 1080–1093.
46 S. Han, Y. Li, F. Hao, H. Zhou, S. Qi, G. Tian and D. Wu, *Eur. Polym. J.*, 2021, **143**, 110206.
47 Y. Wang, S. Wang, C. Bian, Y. Zhong and X. Jing, *Polym. Degrad. Stab.*, 2015, **111**, 239–246.
48 R. Bei, K. Chen, Y. He, C. Li, Z. Chi, S. Liu, J. Xu and Y. Zhang, *J. Mater. Chem. C*, 2023, **11**, 10274–10281.
49 R. Bei, K. Chen, Q. Liu, Y. He, C. Li, H. Huang, Q. Guo, Z. Chi, J. Xu, Z. Chen, S. Liu and Y. Zhang, *Macromolecules*, 2024, **57**, 2142–2153.
50 H. Li, M. R. Gadinski, Y. Huang, L. Ren, Y. Zhou, D. Ai, Z. Han, B. Yao and Q. Wang, *Energy Environ. Sci.*, 2020, **13**, 1279–1286.
51 Z. Pei, Y. Liu, W. Zhao, C. Yang, S. Li, P. Jiang, J. Chen and X. Huang, *Adv. Funct. Mater.*, 2023, **34**, 202307639.
52 J. Li, S. Liu, G. Zhu, C. Lu, Y. Ba, G. Chen and X. Fang, *Eur. Polym. J.*, 2023, **199**, 112439.
53 L. Liu, Y. Duan, H. Yun, X. Chen, J. Liu, S. Lv and Y. Zhang, *Ind. Crops Prod.*, 2024, **220**, 119239.